YTUP

Journal of Thermal Engineering
https://jten.yildiz.edu.tr/
https://doi.org/10.47481/jten.0046

RESEARCH ARTICLE

Design and optimization of an axial turbo-vapor compressor through three- dimensional flow analysis and loss modeling

Mostafa Shawky Abdel Moez[1,*], Amin Mobarak[2]

[1]Department of Mechanical Power Engineering, Faculty of Engineering, Cairo University, 12613 Giza, Egypt
[2]Department of Mechanical Power Engineering, Faculty of Engineering, Cairo University, 12613 Giza, Egypt

Abstract

The novelty of the TVC lies in its integrated axial design, in which a compressor creates a vacuum in the evaporator, thereby lowering the evaporation temperature of water from 100°C to ~85°C. The system is started by an external motor, and once operational, the expansion of vapor in the turbine directly drives the compressor into a self-sustaining loop, thereby eliminating the need for inlet/outlet guide vans and reducing aerodynamic losses and cost. Enhancing TVC efficiency is significant because of its direct impact on system reliability, energy conversion efficiency, and overall operational costs. A comprehensive three-dimensional design and optimization methodology was employed, combining mean-line analysis, blade geometry generation, and detailed CFD simulations using ANSYS CFX. The investigation accounts for real-world loss mechanisms, including incidence and deviation losses, secondary-flow losses, and tip-clearance losses, enabling a realistic performance assessment. The results show that the optimized blade profiles achieve compressor and turbine total-to-total isentropic efficiencies of up to 97.6% and 86.9%, respectively, with a pressure ratio reaching 1.49 and a specific work of approximately 152.5 kJ/kg. Parametric analysis of turbine stagger angle reveals its strong influence on flow uniformity and efficiency, with improper stagger causing measurable degradation due to increased secondary losses. These findings indicate that careful three-dimensional blade optimization substantially enhances TVC performance. The novelty of this work lies in integrating detailed loss modeling with full 3D CFD-based optimization, moving beyond traditional one-dimensional or simplified approaches commonly reported in the literature. The proposed methodology provides a robust design framework for advanced energy and desalination applications.

Keywords: Turbo-Vapor Compressor (TVC); axial compressor, axial turbine, three-dimensional flow, tip clearance, secondary losses, ANSYS CFX, efficiency optimization, stagger angle, blade design

Cite this article as: Abdel Moez, M. S., & Mobarak, A. (2026). Design and optimization of an axial turbo-vapor compressor through three-dimensional flow analysis and loss modeling. Journal of Thermal Engineering, 12(4), 1493–1509. https://doi.org/10.47481/jten.0046

1. Introduction

Turbo-vapor compressors (TVCs) are key components in low-temperature power generation and thermal desalination systems, where overall system performance is highly sensitive to aerodynamic efficiency [1, 2]. The novelty of the TVC lies in its integrated axial design, where a compressor creates a vacuum in the evaporator to lower the water evaporation temperature from 100°C to ~85°C. The system is started by an external motor, and once operational, the expansion of vapor in the turbine directly drives the compressor into a self-sustaining loop, eliminating the need for inlet and outlet guide vanes, thus reducing aerodynamic losses and cost. In such applications, even small efficiency losses can significantly reduce net power output and increase specific energy consumption, limiting the economic viability of these technologies. Axial TVCs operating at moderate pressure ratios are particularly affected by complex three-dimensional flow phenomena, including secondary flows, tip-leakage vortices, end wall losses, and flow separation, which lead to non-uniform outlet conditions and elevated entropy generation.

Conventional one-dimensional and mean-line design methods cannot accurately capture these loss mechanisms, often result-

*Corresponding Author
E-mail Adress: mostafashawky11@cu.edu.eg

Submitted: 24 January 2026; **Accepted:** 29 January 2026

This paper was recommended for publication in revised form by Editor-in-Chief Ahmet Selim Dalkılıç

ing in designs that underperform in realistic operating conditions. Moreover, the influence of key blade geometric parameters, such as stagger angle and three-dimensional blade shaping, has not been sufficiently quantified for axial TVCs. This lack of detailed aerodynamic understanding restricts effective optimization and limits further performance improvements, thereby motivating the need for advanced three-dimensional analysis and design strategies.

In the current work, the effect of other losses that occur in the turbo-vapor compressor and turbine, as mentioned in the literature review [3], will be considered. This work will calculate sources of losses in turbo-vapor compressors, such as end wall, secondary, and profile losses. Actual efficiency will be calculated and compared with the efficiencies predicted in [4, 5]. Sources of turbine losses, including profile, secondary, trailing edge, and blade clearance losses, will be included. These losses have a significant effect on the performance of the turbo-vapor compressor and the turbine, and consequently affect the absolute and relative velocities, the absolute and relative angles, and the work done by the turbine or on the compressor. Moreover, the current work determines the optimal blade shapes for the turbo-vapor compressor and turbine based on the calculated velocities and angles.

2. Compressor three-dimensional design

The present work introduces a comprehensive three-dimensional (3D) design methodology that integrates multiple loss sources beyond profile losses, including:

a. Secondary flow losses due to passage vortices and hub-to-shroud pressure gradients.
b. Tip clearance losses resulting from leakage flows over blade tips.
c. End-wall losses are attributed to annulus boundary layers.
d. Trailing edge and shock losses were applicable.

The modelling of 3D losses in axial compressors and turbines has evolved significantly over the decades. Early semi-empirical models by Howell [6] and Lieblein [7] were extended by Koch & Smith [8]to include compressibility and Reynolds number effects. For turbines, Aungier [9] and Horlock [10] provided consolidated correlations for secondary, tip clearance, and trailing-edge losses. Recent advancements in computational fluid dynamics (CFD) [11, 12, 13]have enabled high-fidelity 3D simulations, yet empirical and semi-empirical models remain indispensable during preliminary design for their computational efficiency and robustness across a wide range of operating conditions.

Advantages of the Adopted Algorithm:

a. The 3D design approach employed in this study combines:
b. Free-vortex design principles to maintain radial equilibrium.
c. Integrated loss models that account for profile, secondary, tip clearance, and end-wall effects simultaneously.
d. Iterative coupling between aerodynamic performance and geometric parameters (solidity, aspect ratio, tip gap).
e. Validation and refinement using ANSYS CFX for 3D flow simulation, ensuring physical consistency and accuracy.

This hybrid methodology strikes a balance between computational cost and predictive accuracy, making it suitable for the preliminary and detailed design phases of the novel TVC. The outcomes of this chapter include final blade geometries, spanwise efficiency distributions, and a parametric assessment of tip clearance and stagger angle effects—all essential for achieving a self-sustaining, low-loss TVC stage.

2. 1. Literature review on compressor losses

A Compressor has different types of losses. Figure 1 shows different types of losses in the compressor. They are related to physical blade properties such as pitch, thickness, throat opening, and fluid incidence. They are also related to the velocity and pressure distributions around the blades, which affect the boundary layers around the blades. The finite thickness of the blade trailing edge may be expected to give rise to pressure losses in the same manner as sudden enlargement of a pipe through which the fluid is flowing.

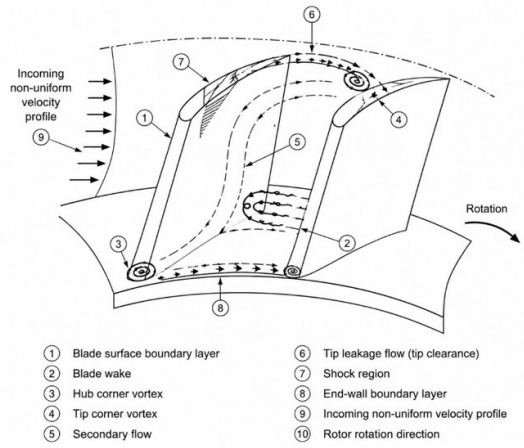

Figure 1. Flow fields in a compressor blade [11]

2.2. Blade profile loss coefficient: Howell work

This paragraph aims to provide a literature review of the correlations available in the open literature concerning the blade profile loss modeling. The first study to mention is the one made by Howell [6]. He tried in 1945 to estimate the loss in terms of the familiar drag and lift coefficients used for aircraft analysis. He defines the drag coefficient for the determination of the efficiency as $CD = CD_p +$

$CD_a + CD_s$, Where CD_p is the profile drag coefficient obtained from cascade tests in wind tunnels, CD_a is the annulus drag coefficient corresponding to friction on the walls of the annulus, and CD_s covers all the secondary losses contribution. The drag coefficient was then related to the pressure loss coefficient. The technique proposed by Howell was then substituted by the work of Lieblein.

2.3. Blade profile loss coefficient : Lieblein work

The studies of S. Lieblein [12] have represented a milestone in the development of empirical correlation models for blade profile loss prediction and modeling. Lieblein introduced two indicators of the blade loading to be used in the loss estimation. Respectively, in 1953 [12], he introduced the definition of the diffusion factor D, and in 1959 [7], he introduced the definition of the equivalent diffusion factor D_{eq}. These factors are functions of the maximum relative flow velocity in the blade passage and functions of the relative inlet velocities. The Lieblein works consider the velocity to be taken relative to the blade. Those definitions in this form are clearly applicable to a rotor blade row, and to be also used for a stator one, the relative velocity ratios have to be substituted by the corresponding absolute velocity ratios. The diffusion factor and the identical diffusion factor were used by Lieblein to estimate the boundary layer momentum thickness, which was then used for the blade profile loss coefficient estimation. The fundamental state of Lieblein's contribution was that he showed that the losses around a blade profile are connected to the boundary layer momentum thickness, and as the aerodynamic loading on a compressor blade increases, the diffusion on the suction surface increases while the diffusion on the pressure side stays approximately constant. The correlations and equations developed by Lieblein were obtained from studies done on purely 2-Dimensional, low-speed cascades with NACA 65 – (A10) and British C4 circular arc blade profiles.

The ratio, $W_{max}/W_{1,}$ is calculated from Equation 1. Equivalent diffusion factors are computed from Equation 2 [3, 12]. Using relative velocity at the inlet and exit, solidity, and profile loss coefficient can be calculated using Equation 3 [3, 12] Figure 2 shows the basic compressor velocity triangle and how angles are measured.

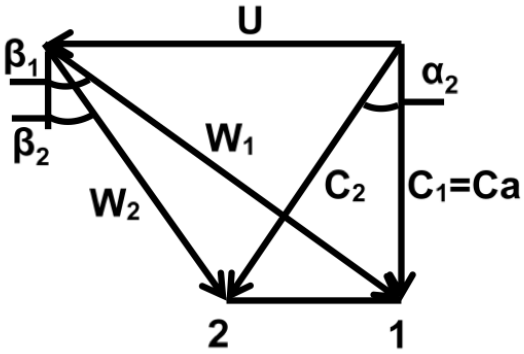

Figure 2. Basic compressor velocity triangle

$$\left(\frac{W_{max}}{W_1}\right) = 1.12 + 0.61\frac{\cos^2\beta_1}{\sigma}[\tan\beta_1 - \tan\beta_2] \quad \text{Equation 1}$$

$$D_{eq} = \left(\frac{W_{max}}{W_1}\right)^{\frac{W_1}{W_2}} \quad \text{Equation 2}$$

$$\frac{Y_t\cos\beta_2}{2\sigma}\left(\frac{W_1}{W_2}\right)^2 = K_1[K_2 + 3.1(D_{eq} - 1)^2 + 0.4(D_{eq} - 1)^8] \quad \text{Equation 3}$$

$$K_2 = 1 + (\bar{s}/\bar{h})\cos\beta_2 + 0.04K_{RE}/K_1 \quad \text{Equation 4}$$

3. Theory

3.1. Compressor exit properties and velocities calculations

All required compressors' exit properties were calculated as mentioned in using the total loss coefficient instead of the profile loss coefficient.

3.2. Global output parameters of compressor

After the specific work has been calculated and all velocities have been determined at the mean section, the free vortex can be used to determine these velocities at the hub and tip sections, as discussed in previous work. The same procedure used for the mean section will be applied to calculate the deflection and camber angles for the hub and tip sections. Moreover, thermodynamic properties can be calculated for the three sections, as described in the previous work. Table 1 includes all inputs used in the three-dimensional calculations of the compressor at the specified mass flow rate.

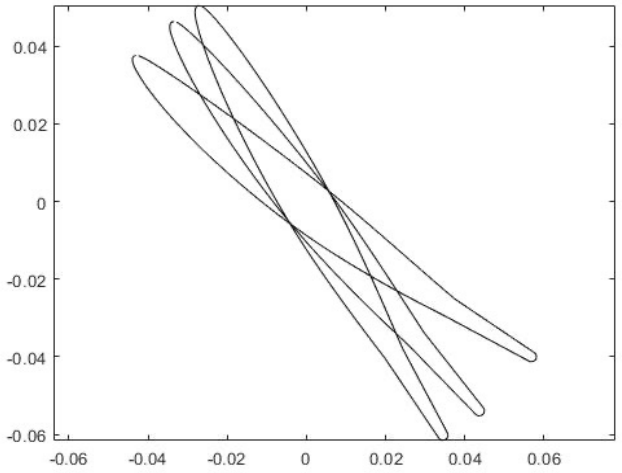

Figure 3. Figure 3 shows compressor blade (of type NACA-65) profiles at three sections through the compressor from the hub, mean, and tip with different calculated stagger angles based on different losses, incidence, and deviation angles of the compressor blades

Table 1. General inputs for compressor three-dimensional calculations

Parameter	Value	unit
Total temperature at the inlet (T_{o1})	83.3181	C
Mass flow rate (m)	50	kg/s
Revolution per minute	3000	Rpm
Hub to tip ratio	0.5	
Flow coefficient at the hub section	1	
Initial aspect ratio	3	
Tip gap	0	
Deceleration ratio (W_2/W_1)	0.85	
Initial solidity at hub section (σ_h)	0.85	
Solidity at tip section (σ_t)	$\sigma_h \times (D_h/D_t)$	
Solidity at mean section (σ_m)	$\sigma_m \times (D_h/D_m)$	
Location of max camber normalized by the chord of the compressor	0.5	
Maximum thickness to chord ratio	0.1	
Blade shape parameter constant (K_{sh})	1	

Table 2 summarizes the global outputs resulting from three-dimensional calculations mentioned earlier in the current work section 5.2. These parameters are general over the compressor, such as the number of blades (Z), chord (C), aspect ratio (AR), height (H), hub diameter (D_h), mean diameter (D_m), tip diameter (D_t), specific work (W), and efficiency (η). All parameters are the same as for two-dimensional flow calculations, except for the efficiency (η), which decreased from 94.63% in two-dimensional calculations to 93.5% in three-dimensional calculations under the same dimensions and operating conditions.

Table 2. Global outputs result from compressor three-dimensional calculations

Parameter	Value	Unit
Number of blades (Z)	18	
Chord (c)	0.1126	M
Aspect ratio (AR)	3.182	
Blade height (H)	0.3583	M
Hub diameter (D_h)	0.7166	M
Mean diameter (D_m)	1.0749	M
Tip diameter (D_t)	1.4333	M
Specific work (W)	4895.18	J/kg
Efficiency (η)	0.935	

Properties and Velocities at Hub Mean and Tip Sections of Compressor

Table 3 summarizes computed properties and velocities from three-dimensional calculations at the hub section; Table 4 summarizes those at the mean section. Table 5 summarizes the computed properties and velocities derived from three-dimensional calculations at the tip section. In the mean section, the incidence decreased from 0.65 degrees in two-dimensional calculations to 0.62 degrees in three-dimensional calculations. An increase in deviation of about 0.04 degrees and a decrease in stagger of about 0.02 degrees is observed between two-dimensional and three-dimensional calculations at the mean section. The differences between 2D and 3D results are small because the secondary losses are negligible in the mean section. Efficiency decreased from hub to tip because the loss model was based on the relative velocity, which increased from hub to tip. Efficiency for compressors is like values mentioned by [6, 8, 16].

In the present 3D design methodology:

- Compressor losses were modeled using Lieblein's diffusion factor approach with $K_1 = 1.0$ and $K_2 = 2.0$
- Turbine losses followed Aungier's correlations with $K_s = 0.035$ and $K_{tc} = 1.1$.
- Secondary loss constants were calibrated against CFD results to ensure consistency with ANSYS CFX predictions.
- Tip clearance analysis used m = 0.75 for both compressor and turbine.

These constants were integrated into an iterative loss-prediction loop within the MATLAB design code, ensuring that blade geometry updates reflected realistic loss increments across spanwise sections.

Table 3. Summary of computed properties and velocities based on three-dimensional calculations at the compressor hub section

Hub Section output		
Parameter	Inlet	Exit
Total temperature (C)	83.85	86.48
Total pressure (Bar)	0.50	0.51
Total enthalpy (kJ/kg)	2650.37	2655.26
Entropy (kJ/kg.K)	7.6110	7.6126
U (m/s)	121.26	121.26
Ca (m/s)	121.26	118.88
Cu (m/s)	0.00	40.37
C (m/s)	121.26	127.80
Wu (m/s)	121.26	80.89
W (m/s)	171.49	145.76
β (degree)	45.00	33.71
α (degree)	0.00	18.76
Incidence (degree)	0.13	
Deviation (degree)	4.19	
Stagger (degree)	37.52	
Chord(m)	0.128	
Efficiency (%)	96.8	

Table 4. Summary of computed properties and velocities based on three-dimensional calculations at the mean section

Mean Section output		
Parameter	Inlet	Exit
Total temperature (C)	83.85	86.48
Total pressure (Bar)	0.50	0.51
Total enthalpy (kJ/kg)	2650.37	2655.26
Entropy (kJ/kg.K)	7.6110	7.6126
U (m/s)	181.89	181.89
Ca (m/s)	121.26	118.88
Cu (m/s)	0.00	26.91
C (m/s)	121.26	121.88
Wu (m/s)	181.89	154.98
W (m/s)	218.60	196.78
β (degree)	56.31	51.96
α (degree)	0.00	12.76
Incidence (degree)	0.62	
Deviation (degree)	3.44	
Stagger (degree)	52.15	
Chord (m)	0.128	
Efficiency (%)	96.04	

Table 5. Summary of computed properties and velocities based on three-dimensional calculations at the tip section

Tip Section output		
Parameter	Inlet	Exit
Total temperature (C)	83.85	86.48
Total pressure (Bar)	0.50	0.51
Total enthalpy (kJ/kg)	2650.37	2655.26
Entropy (kJ/kg.K)	7.6110	7.6126
U (m/s)	242.52	242.52
Ca (m/s)	121.26	118.88
Cu (m/s)	0.00	20.18
C (m/s)	121.26	120.57
Wu (m/s)	242.52	222.33
W (m/s)	271.14	253.25
β (degree)	63.43	61.39
α (degree)	0.00	9.64
Incidence (degree)	1.11	
Deviation (degree)	2.31	
Stagger (degree)	60.70	
Chord(m)	0.128	
Efficiency (%)	94.64	

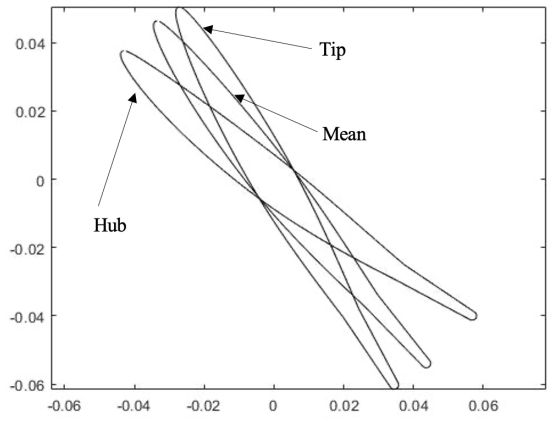

Figure 4. Compressor NACA-65 profiles at three sections of turbo-vapor compressor

4. Turbine three-dimensional design

4.1. Turbine secondary and profile losses

Turbine losses, as mentioned in the literature review, are profile, secondary, tip gap, and end-wall losses. Horlock [13]includes some basic correlations for loss calculations in the axial turbines. Turbine total losses are calculated, which is used for low-angle deflection blades and implies appropriate efficiency values at different turbine sections, while the profile loss coefficient is calculated [13] , where ζ_p is the profile losses, and H/b is the aspect ratio. Tip gap losses are assumed to be zero at first, then a parametric study shall be done to deduce their effect on TVC works and efficiencies.

4.2. Global output parameters of turbine in turbo-vapor compressor

The Total enthalpy at the turbine exit can be calculated from the local exit enthalpy and axial velocity; the stagnation pressure at the exit can then be determined from steam tables using the total exit enthalpy and total exit entropy. The isentropic total enthalpy at the exit can be determined from steam tables, using the exit stagnation pressure and the inlet total entropy. Efficiency can be calculated as the ratio of the actual total enthalpy drop to the isentropic total enthalpy drop. The specific work done can be calculated as the difference between the total enthalpy at the exit and at the inlet.

After the specific work is obtained and all velocities are determined at the mean section, the free vortex can be used to calculate these velocities at the hub and tip sections, as discussed in Section 4.4. The procedure applied to the mean section will be used to calculate the deflection and camber angles for the hub and tip sections. Moreover, thermodynamic properties can be calculated in three distinct ways, as discussed in previous work. Table 6 includes all inputs used for three-dimensional calculations of the turbine at the specified mass flow rate.

Figure 4 shows turbine blade (of type A3K7) profiles at three different sections through the turbine from hub to tip with different calculated stagger angles based on different losses, incidence, and deviation angles of the turbine blades.

Table 6. General input for turbine three-dimensional calculations

Parameter	Value	Unit
Total temperature at the inlet (T_{o2})	86.48	C
Mass flow rate (m)	50	kg/s
Revolution per minute	3000	Rpm
Hub to tip ratio	0.5	
Flow coefficient at the hub section	1	
Initial aspect ratio	3	
Initial tip gap	0	
Solidity at hub section (σ_h)	1.05	
Solidity at tip section (σ_t)	$\sigma_h(D_h/D_t)$	
Solidity at mean section (σ_m)	$\sigma_m(D_h/D_m)$	
Turbine thickness to chord ratio	0.2	
A3K7 TE radius thickness	1% chord	

Table 7 summarizes the global outputs resulting from the three-dimensional calculations mentioned earlier in the current work. These Parameters are general over the turbine, such as the number of blades (Z), chord (c), aspect ratio (AR), height (H), hub diameter (D_h), mean diameter (D_m), tip diameter (D_t), specific work (W), efficiency (η), and pressure ratio (PR). Turbine Efficiencies are similar to those mentioned by [9, 17]

Table 7. Global outputs result for turbine in tvc three-dimensional calculations

Parameter	Value	Unit
Number of blades (Z)	18	
Chord (c)	0.1415	M
Aspect ratio (AR)	2.53	
Height (H)	0.3583	M
Hub diameter (D_h)	0.7166	M
Mean diameter (D_m)	1.0749	M
Tip diameter (D_t)	1.4333	M
Specific work (W)	4895.18	J/kg
Efficiency (η)(%)	92.56	

4.3. Properties and velocities at hub, mean, and tip sections of turbine

Tables 8,9, and 10 show the local outputs at the hub, mean, and tip sections, respectively. For the mean section, the deviation decreased from 0.2854 degrees for two-dimensional calculations to 0.28 degrees for three-dimensional calculations. Stagger 0.08-degree difference between two-dimensional and three-dimensional calculations at the mean section. Efficiency decreased from hub to tip because the loss model was based on the relative velocity, which increased from hub to tip.

Table 8. Summary of computed properties and velocities based on three-dimensional calculations at hub section for turbine in TVC

Hub Section output		
Parameter	Inlet	Exit
Total temperature (C)	86.48	83.29
Total pressure (Bar)	0.51	0.49
Total enthalpy (kJ/Kg)	2655.26	2649.40
entropy (kJ/kg.K)	7.6126	7.6167
U (m/s)	121.26	121.26
Ca (m/s)	118.88	122.87
Cu (m/s)	40.37	0.00
C (m/s)	127.80	122.09
Wu (m/s)	80.89	121.26
W (m/s)	145.76	172.07
β (degree)	33.71	44.62
α (degree)	18.76	0.00
Incidence	0.00	
Deviation	0.76	
Stagger	39.91	
Chord (m)	0.1415	
Efficiency (%)	88.73	

Table 9. Summary of Computed Properties and Velocities Based on Three-Dimensional Calculations at Mean Section for Turbine in TVC

Mean Section output		
Parameter	Inlet	Exit
Total temperature (C)	86.48	83.29
Total pressure (Bar)	0.51	0.49
Total enthalpy (kJ/kg)	2655.26	2649.40
entropy (kJ/kg.K)	7.6126	7.6167
U (m/s)	181.89	181.89
Ca (m/s)	118.88	122.87
Cu (m/s)	26.91	0.00
C (m/s)	121.88	122.87
Wu (m/s)	154.98	181.89
W (m/s)	196.78	219.50
β (degree)	51.96	55.96
α (degree)	12.76	0.00
Incidence	0.00	
Deviation	0.28	
Stagger	54.36	
Chord (m)	0.1415	
Efficiency (%)	83.79	

Table 10. Summary of Computed Properties and Velocities Based on Three-Dimensional Calculations at Tip Section for Turbine in TVC

Tip Section output		
Parameter	Inlet	Exit
Total temperature (C)	86.48	83.29
Total pressure (Bar)	0.51	0.49
Total enthalpy (kJ/kg)	2655.26	2650.37
entropy (kJ/kg.K)	7.6126	7.6167
U (m/s)	242.52	242.52
Ca (m/s)	118.88	122.87
Cu (m/s)	20.18	0.00
C (m/s)	120.57	122.87
Wu (m/s)	222.33	242.52
W (m/s)	253.25	271.87
β (degree)	61.39	63.13
α (degree)	9.64	0.00
Incidence(degree)	0.00	
Deviation(degree)	0.09	
Stagger(degree)	62.51	
Chord (m)	0.1415	
Efficiency (%)	82.7	

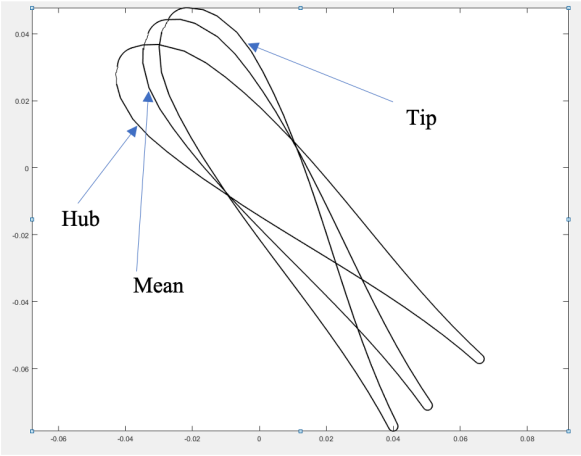

Figure 5. Turbine A3K7 profiles at three sections for turbo-vapor compressor

5. CFX mesh independence test and validation

Mesh independence analysis is conducted to select the most accurate and economic mesh size. First, the turbine work calculated from the coarse mesh simulation is 4793 J/kg, and the difference from the calculated work of 102.1 J/kg with an elapsed time of 1.1 hours. Medium mesh results in a turbine work difference between calculated and simulated of 60.1 J/kg for 3.75 hours. Finally, fine mesh size predicts a net difference in work of 52.1 J/kg with an elapsed time of 12 hours, as shown in Table 11. Medium mesh size is selected due to its less computational time and close accuracy for the mesh. Shear Stress Transport (SST) kω model, which is the default and most widely validated turbulence model in ANSYS CFX for turbomachinery applications [17, 18, 19]

Table 11. Mesh independence analysis results

Number of Nodes	Calculations Turbine Work(J/kg)	Simulation Turbine Work(J/kg)	%of Turbine Work	Time Elapsed(hr)
416208	4895.1	4793	2.08	1.1
1179282	**4895.1**	**4835**	**1.22**	**3.75**
2469090	4895.1	4843	1.06	12

Experimental Benchmark Description

The NASA Rotor 37 test case was selected for validation due to its comprehensive ex- perimental database and status as an industry-standard benchmark for transonic axial compressor CFD validation [20, 21]. The experimental data were obtained from the NASA Glenn Research Center's Low-Speed Axial Compressor Facility.Results are shown in Table 12 and Figure 5.

Table 12. CFD validation

Parameter	Experimental	CFD	Absolute Error	Relative Error
Peak pressure ratio	2.106	2.086	-0.020	0.95%
Peak efficiency (%)	88.5	87.4	-1.1 pp	1.24%
Choke mass flow (kg/s)	20.93	20.76	-0.17 kg/s	0.81%
Stall margin (%)	12.3	11.8	-0.5 pp	4.07%

Notes: pp = percentage points. All errors are within acceptable limits for RANS-based CFD: pressure ratio ≤2%, efficiency ≤2%, and mass flow gap of 1.5%. The slight underprediction of efficiency (1.24%) is consistent with the behavior of the SST k − ω model for transonic compressors.

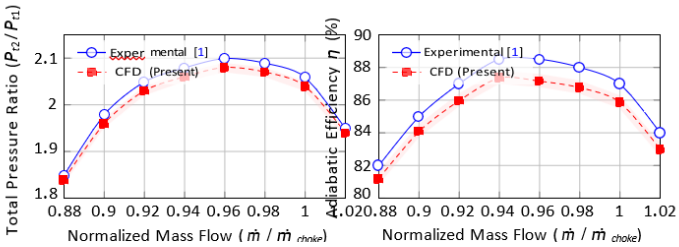

Figure 6. Validation of CFD methodology against NASA Rotor 37 experimental data

The validation employed the same solver settings, turbulence model, and mesh quality as those used in the subsequent TVC analysis. (a) Total pressure ratio characteristics showing excellent agreement across the operating range. (b) Adiabatic efficiency characteristics with CFD predictions within 1.3% of experimental values. The shaded regions represent CFD uncertainty bounds from grid convergence analysis.

6. Grid convergence and uncertainty quantification

A formal Grid Convergence Index (GCI) analysis was performed following the methodology of [22]to quantify numerical uncertainty:

Table 13. Grid Convergence Index analysis for validation case

Parameter	Fine Grid	Medium Grid	Coarse Grid	GCI (%)
Nodes per passage	2,469,090	1,179,282	416,208	–
Total pressure ratio	2.088	2.086	2.081	0.34
Adiabatic efficiency (%)	87.45	87.42	87.35	0.11
Mass flow rate (kg/s)	20.77	20.76	20.72	0.24
Computation time (hours)	12.0	3.75	1.1	–

The GCI for key parameters was below 0.35%, confirming that the medium grid (1.18 million nodes) provides grid-independent solutions with acceptable computational cost.

7. TVC tip clearance analysis on CFX for three-dimensional design

As shown in the previous section, MATLAB code was used to generate output profiles for the compressor and turbine, with profile and secondary losses included. When simulating these profiles in CFX, compressor work exceeded turbine work by 106 J/kg at zero tip gap (about 2% of the work). A tip gap analysis will be conducted on the compressor and turbine blades of the TVC to select the tip gap that minimizes the work difference between the compressor and the turbine. This tip gap is necessary for the manufacture of compressor and turbine blades for TVC. Table 11 shows the effect of tip-gap variation on compressor and turbine work. As the tip gap increases, the difference in work between the TVC compressor and turbine increases, starting from 152.5 J/kg (3% of work) at a 1 mm tip gap and reaching about 327 J/kg at a 20 mm tip gap, which is relevant for manufacturing operations. Consequently, a tip gap of 1 mm will be selected to minimize the compressor and turbine work of TVC. The tip gap reduces the work for the turbine and compressor because of losses it causes.

Table 14. Tip clearance analysis for TVC using ANSYS CFX

Tip Clearance (mm)	Tip Clearance (%h)	W_c(J/kg)	W_t(J/kg)	W_c-W_t(J/kg)	W_c-W_t (% W_t)
0	0	5843.25	5736.5	106.75	1.86
1	**0.13**	**5854.5**	**5702**	**152.5**	**2.67**
3	0.39	5835	5670	165	2.91
5	0.65	5833.5	5646	187.5	3.32
7	0.9	5827	5636.5	190.5	3.37
10	1.3	5815	5608	207	3.69
20	2.6	5783.75	5456.75	327	5.99

The selected 1 mm tip gap (0.28% of blade height) represents an optimal balance between aerodynamic performance and mechanical feasibility. Industrial axial turboma- chinery typically employs 0.5–2.0% tip clearances [22], corresponding to 1.79–7.16 mm for H = 0.358 m. The 1 mm value considers:

- Aerodynamics: Minimizes leakage losses while maintaining work balance

- Manufacturing: Within CNC machining and precision casting capabilities
- Operation: Accommodates centrifugal growth (~0.3 mm at 3000 RPM) and ther- mal expansion
- Safety: Provides ~0.5 mm margin for transients and assembly

For sustained operation, active clearance control systems [6] could maintain this op- timal gap.

8. TVC Parametric Study for Three-Dimensional Design Using CFX

When simulating the TVC blade profiles generated by MATLAB in CFX, the compressor work was 106 J/kg higher than the turbine work at zero tip gap. A tip-gap analysis was conducted on the compressor and turbine blades of TVC to identify the tip gap that minimizes the work difference between the compressor and turbine. A tip-gap value of 1 mm was selected to minimize the difference between the compressor and turbine work of the TVC, resulting in a higher compressor work of 152.5 J/kg, i.e., 3% of the specific work. In this section, the difference between compressor and turbine work will be minimized while ensuring turbine work remains slightly greater than compressor work to avoid fluctuations in the cycle. Turbine stagger will be rotated by a few degrees clockwise for negative values and a few degrees counterclockwise for positive values to achieve the required optimum configuration. Table 12 shows the effect of turbine stagger rotation on compressor and turbine work and efficiencies. The parametric study was conducted by rotating the turbine stagger about the blade centroid line from -4 degrees to 8 degrees in 1-degree steps to determine the smallest difference in work between the compressor and turbine of the TVC. Table 12 shows that at a -4-degree turbine stagger, the difference was substantial (about 5035 J/kg, with compressor work exceeding turbine work). Moreover, as the stagger angle increased (i.e., in the positive direction), the turbine work output increased. For positive-direction rotation, stagger rotation was conducted from one to eight degrees, resulting in a work difference ranging from 1184.5 J/kg at a one-degree stagger rotation to 9364.25 J/kg at 8 degrees; therefore, stagger rotation values greater than one degree were rejected. Consequently, the turbine stagger rotation determined by the analysis will be less than one degree. A turbine stagger rotation of 0.1493 degrees will be selected, with turbine work 6.5 J/kg greater than compressor work (0.1% of the work) and compressor and turbine efficiencies of 97.6 % and 86.9 %, respectively. The stagger angle of the turbine affects turbine work; many values were tested in CFX with different steps, and here some are shown. All efficiencies are total-to-to-total isentropic (ηtt). The compressor efficiency of 97.6% aligns with values reported for optimized low-pressure-ratio single-stage axial compressors: [24]reports ηtt > 94% for research compress- sores, while [23] notes 92-95% for industrial designs.

Table 15. Turbine Stagger rotation effect on compressor and turbine work and efficiencies

γ_T(Degree)	W_C(J/kg)	W_T(J/kg)	W_T-W_C(J/kg)	η_C	η_T
-4	5986.75	951.5	-5035.3	0.97662	0.61698
-3	5968.5	2036.25	-3932.3	0.97643	0.75393
-2	5946.5	3181.25	-2765.3	0.97599	0.81036
-1	5931	4425.75	-1505.3	0.97593	0.84281
0.05	5918.25	5776.25	-142	0.97597	0.86688
0.1	5918.75	5853.25	-65.5	0.97591	0.86801
0.14	**5918**	**5924.5**	**6.5**	**0.97594**	**0.86893**
0.15	5917.75	5925.75	8	0.97593	0.86898
0.15	5909.75	5951	41.25	0.89575	0.719192
0.15	5909.75	5951	41.25	0.89575	0.719192
0.2	5917	5978.75	61.75	0.97587	0.86973
0.25	5916.25	6050.5	134.25	0.97593	0.87072
0.3	5915.5	6135.5	220	0.97593	0.87163
0.35	5915.75	6184.25	268.5	0.9759	0.87241
0.4	5915.25	6273.5	358.25	0.97586	0.87348
0.45	5914	6349.25	435.25	0.97595	0.87433
0.5	5913.75	6416	502.25	0.97589	0.87509
1	5908.5	7093	1184.5	0.9759	0.88249
2	5900.75	8558.5	2657.75	0.97572	0.89382
3	5893.5	10082.3	4188.8	0.97587	0.89912
4	5882.25	10598.3	4716.05	0.9757	0.86936
5	5889	12842.5	6953.5	0.97582	0.88404
6	5873	13571.8	7698.8	0.97423	0.8523
7	5858.5	14125.3	8266.8	0.97662	0.83257
8	5838.25	15202.5	9364.25	0.97486	0.82117

9. CFX three-dimensional simulation results for final tvc design model

ANSYS CFX 20 [14] is used to examine different parameters for the 1 mm selected tip gap and 0.1493-degree turbine stagger. The investigation was conducted under the following operating conditions: mass flow rate of 50 kg/s; rotational speed, 3000 RPM; the same calculated hub, mean, and tip diameters; static inlet temperature of 80° C; saturated pressure; and the same solidity at the span sections of 2 %, 10 %, 50%, 90 %, 98 %. The selected axial gap is 21% of the compressor chord. Moreover, the circumferential turbine shift is 16 degrees, and the output compressor work estimated from the three-dimensional simulation is 5918 J/kg and 5924.5 J/kg, with the difference in work estimated at 6.5 J/kg (0.1% of work). Figure 5shows the variation of radial velocity along streamwise at 2 % span. Radial velocity resulting from wakes or vortices imposed on the axial flow through the TVC, as the flow exits the trailing edge of the compressor, is not directed toward the leading edge of the turbine, resulting in increased wakes and vortices across the turbine blade. At the second half of the turbine blades, the maximum radial velocity for a 2% span is -5.8 m/s (4.5% of the axial velocity). At the same time, the maximum radial velocity on the compressor blades at a 2 % span is 2 m/s (only 1.6 % of the axial velocity), which indicates that compressor losses are much lower than turbine losses.

Figure 6 shows the variation of radial velocity along the streamwise direction at 10% span. Radial velocity was induced by a wake or vortex imposed on the axial flow through the TVC. The maximum radial velocity over a 10% span, observed in the second half of the turbine blades, is -5.9 m/s (4.8% of the axial velocity). At the same time, the maximum radial velocity at the compressor blades at 10% span is 1 m/s (only 1% of the axial velocity), which indicates that the losses in the compressor are much lower than those in the turbine.

Figure 7 shows the variation of radial velocity along the streamwise direction at 50% span. Radial velocity resulted from a wake or vortex imposed on axial flow through TVC. The maximum radial velocity at 50% span is -6 m/s (only 4.9% of the axial velocity) at the exit of the turbine blades. The maximum radial velocity on the compressor blades at 50% span is 2 m/s (1.6% of the axial velocity only), which indicates that the losses in the compressor are always much lower than those in the turbine.

Figure 8 shows the variation in radial velocity along the streamwise direction at 90% span. Radial velocity resulted from a wake or vortex imposed on axial flow through TVC. The maximum radial velocity at a 90 % span is -1.2 m/s (only 1 % of the axial velocity) at the exit of the turbine blades. At the same time, the maximum radial velocity at the compressor blades at 90% span is 0.8 m/s (only 0.65% of the axial velocity), indicating that compressor losses are much lower than turbine losses. Figure 9 shows the variation of radial velocity in the streamwise direction at 98% span. Radial velocity resulted from a wake or vortex imposed on axial flow through TVC. The maximum radial velocity at 98% span is -3.2 m/s (only 2.6% of the axial velocity) at the exit of the turbine blades. At the same time, the maximum radial velocity at the compressor blades at 98% span is 1 m/s, which is only 0.8% of the axial velocity.

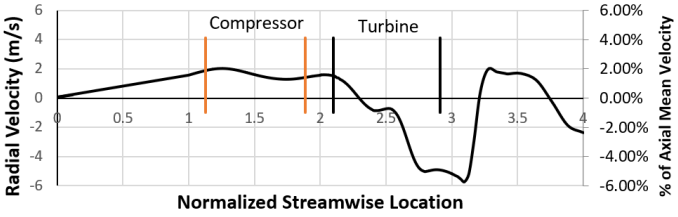

Figure 7. Variation of radial velocity along the streamwise direction at 2% span of the turbo-vapor compressor stage. Radial velocities, normalized to the local axial velocity, indicate secondary flow losses

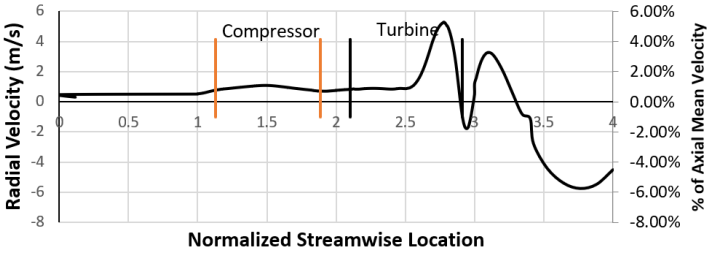

Figure 8. Variation of radial velocity along the streamwise direction at 10% span of the turbo-vapor compressor stage. Velocities are normalized by the local axial velocity to highlight wake and vortex effects

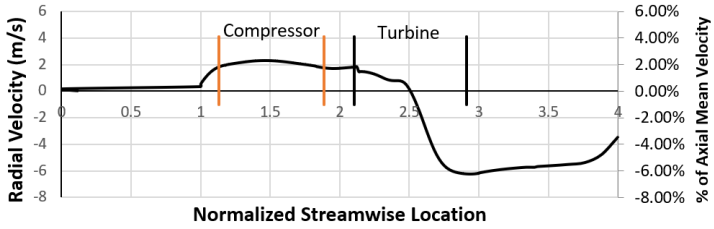

Figure 9. Variation of radial velocity along the streamwise direction at the mid-span (50% span) of the turbo-vapor compressor stage. Radial velocity magnitudes are presented as a percentage of the axial velocity

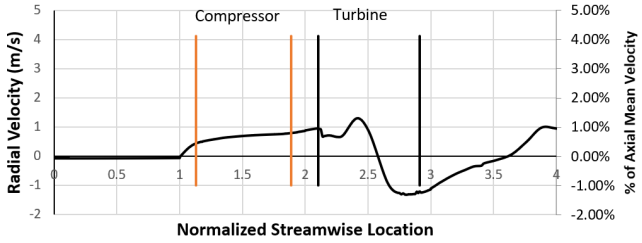

Figure 10. Variation of radial velocity along the streamwise direction at 90% of the turbo-vapor compressor stage. Values are normalized by axial velocity to illustrate secondary flow behavior near the tip

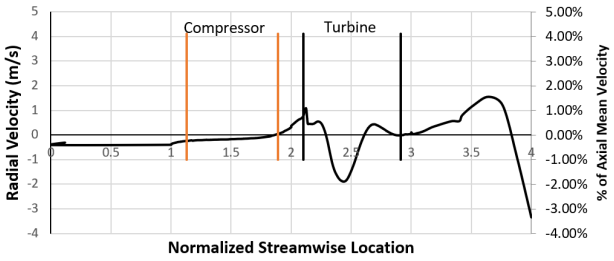

Figure 11. Variation of radial velocity along the streamwise direction at 98% span of the turbo-vapor compressor stage. Normalized radial velocities indicate wake interactions near the blade tip

Figure 11 shows velocity contours for TVC at the 1% spanwise section. Due to the low stagger at the hub, the compressor wake is shifted toward the turbine pressure surface, leading to viscous mixing between the wake and the lower-momentum flow near the pressure side. This explains the relatively low hub axial velocity downstream of the compressor, as shown in Figure 10. Downstream of the turbine, the flow near the hub is slightly accelerated compared with the mean section due to the proximity of the turbine throat to the compressor wake.

Near the tip section, the compressor wake penetrates the higher-momentum region adjacent to the suction surface of the turbine blades, as shown in Figure 11 (velocity contours at 99% span). This high-momentum region of the turbine passage energizes the compressor wake and thereby explains the relatively higher axial flow velocity at the tip downstream of the compressor (Figure 12). Downstream of the turbine, the rate of axial-velocity increase near the tip is slightly lower than near the hub because the turbine throat lags the wake in the tip region.

The reduction in the axial velocity around the mean section downstream of the turbine is attributed to mixing between the compressor wake and the medium-momentum region of the turbine-passage core flow. The turbine blade throat lags the wake (relative to the hub), which delays the process of wake stretching. The path of viscous mixing is longer at the mean section than at the hub section. The maximum variation of axial velocity along span is less than 4% of the average axial velocity.

At the compressor inlet, a slight flow acceleration is observed from the hub to the tip. The high-velocity region on the blade suction surface predominates because the high stagger angle at the tip increases the axial velocity in this section. The total pressure imposed at the inlet boundary allows the static pressure field to influence the velocity field.

Figure 14 shows a streamlined view of TVC at five positions: 2%, 10%, 50%, 90%, and 99%. A Radial shift along the streamline indicates the losses at that location.

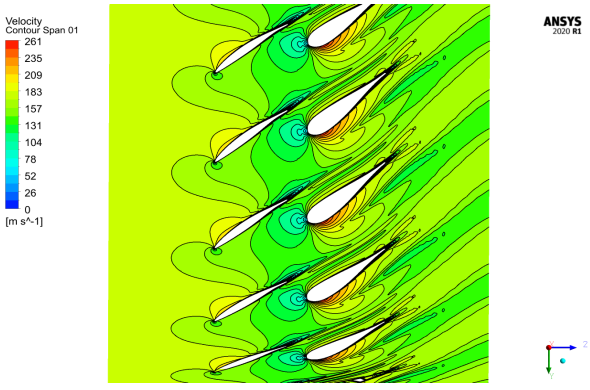

Figure 12. Velocity contours for the turbo-vapor compressor stage at 1% span. Colors represent the absolute velocity magnitude (m/s)

The compressor wake is visible as it interacts with the turbine pressure surface

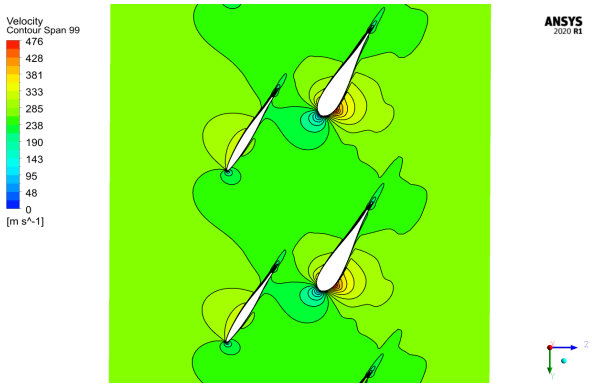

Figure 13. Velocity contours for the turbo-vapor compressor stage at 99% span. Colors represent absolute velocity magnitude(m/s). High-momentum regions near the turbine suction surface energize the compressor wake

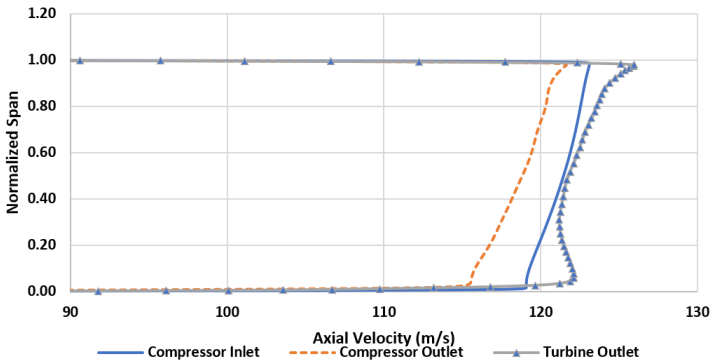

Figure 14. Axial velocity distribution along the span at three axial locations: upstream of the compressor, between the compressor and turbine, and downstream of the turbine. Velocities are normalized by the area-averaged axial velocity

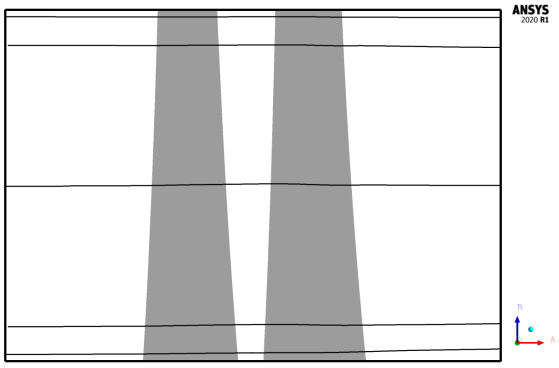

Figure 15. Streamline visualization of the turbo-vapor compressor stage at five spanwise locations: 2%, 10%, 50%, 90%, and 99%. Streamline curvature indicates secondary flow and mixing losses

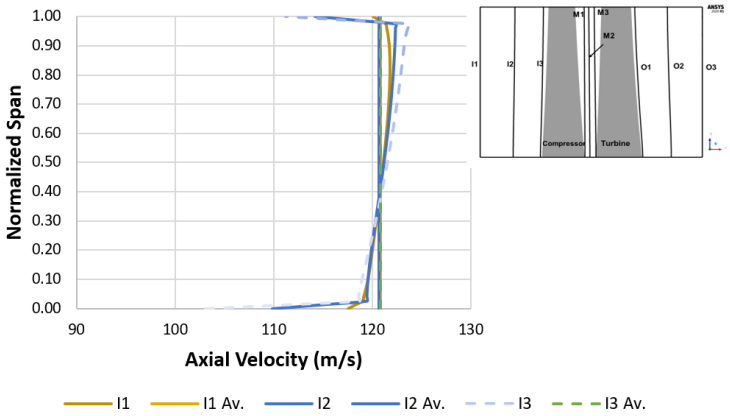

Figure 16. Axial velocity distribution along the span at the compressor inlet for three different axial positions approaching the blade leading edge. Velocities are normalized by the inlet axial velocity

Figure 15 shows axial velocity along the span at three locations of the TVC at the compressor inlet, with a maximum compressor variation of 2-4 %. At the compressor inlet section, which is represented on the chart as three different lines, the location approaches the compressor blade, and axial velocity increases.

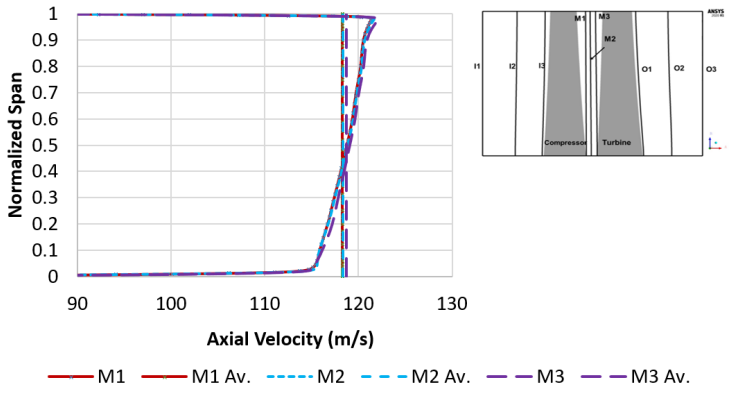

Figure 17. Axial velocity distribution along the span downstream of the compressor at three axial locations. Velocities are normalized by the compressor exit axial velocity

Figure 16 shows axial velocity along the span at three locations in the TVC downstream of the compressor, with a maximum compressor variation of 2–4%. Near the compressor trailing-edge area, maximum values were observed between every two blades of the compressor. At the turbine inlet, the area between the blades was maximal and axial velocity increased.

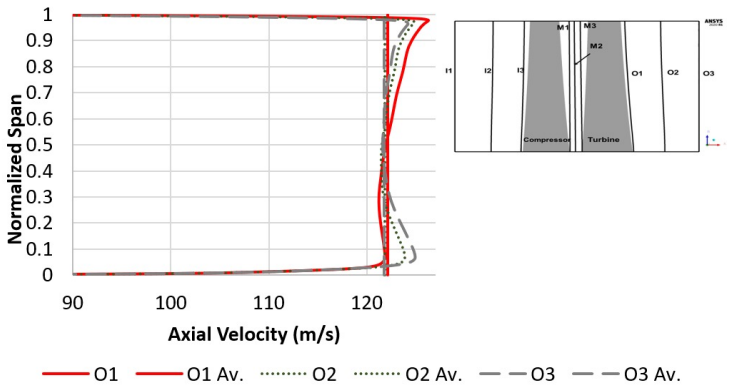

Figure 18. Axial velocity distribution along the span downstream of the turbine at three axial locations. Velocities are normalized by the axial velocity at the turbine exit

Figure 17 shows axial velocity along the span at three locations in the TVC following a maximum compressor variation of 2-4 %. At the turbine exit section, which is represented on the chart by three lines, axial velocity increased with increasing distance from the turbine because the vapor's specific volume increased at constant mass flow rate and area.

10. Interpretation of radial velocity variations in the TVC stage

The radial velocity distributions presented in Figures 5–9 offer critical insight into the three-dimensional flow behavior and secondary loss mechanisms within the TVC stage. Unlike purely axial flow, which is ideal for efficiency, radial velocity components arise from spanwise pressure gradients, blade-to-blade loading, and tip clearance effects. These radial motions are indicative of secondary flow vortices and cross-passage migration, which contribute directly to entropy generation and efficiency degradation.

11. Physical origin of radial velocity

In an axial turbomachine, radial velocity V_r is primarily driven by:

1. Spanwise Pressure Gradients: The radial equilibrium condition is disturbed by blade loading and annulus geometry, leading to radial migration of fluid particles from high-pressure regions (near the hub) to low-pressure regions (near the tip), or vice versa.
2. Tip Clearance Vortices: At the blade tip, leakage flow over the clearance gap rolls up into a vortex with strong radial and tangential velocity components.
3. Passage Vortices: Secondary flows driven by the turning of the endwall boundary layers result in counter-rotating vortices that transport low-momentum

fluid radially across the passage.

4. Wake–Rotor Interaction: The impingement of compressor wakes on the downstream turbine blades can induce local radial velocity fluctuations due to non-uniform momentum exchange.

12. Spanwise variation and loss implications

The results show that radial velocity magnitudes are highest in the turbine section (up to −6 m/s at mid-span), which corresponds to approximately 5% of the axial velocity. In contrast, the compressor exhibits lower radial velocities (~2 m/s, ≤1.6% of axial velocity). This disparity is physically consistent with the higher turning angles and stronger secondary flows typically encountered in turbines than in compressors.

- Hub Region (2–10% span): The negative radial velocity (inward flow) observed in the turbine (Fig. 5–6) suggests the presence of a passage vortex drawing fluid toward the hub. This is compounded by the compressor wake impinging on the pressure side, which enhances mixing and losses near the end wall.
- Mid-Span Region (50% span): The peak radial velocity here (−6 m/s) indicates strong cross-passage migration due to blade loading and the delayed stretching of the compressor wake within the turbine passage. The longer mixing path at mid-span increases viscous dissipation.
- Tip Region (90–98% span): Radial velocities near the tip are influenced by tip leakage vortices and the interaction between the compressor wake and the high-momentum suction-side flow of the turbine. The energization of the wake by the turbine suction surface reduces radial migration but enhances unsteady mixing losses [25-28].

13. Connection to efficiency losses

The magnitude and distribution of radial velocity directly correlate with secondary kinetic energy, which is ultimately dissipated as heat. The area-integrated secondary kinetic energy can be expressed as:

$$E_{secondary} = \frac{1}{2}\rho \int (V_r^2 + V_\theta'^2)\, dA \qquad \text{Equation 5}$$

where V_θ' is the deviation from the mean tangential velocity. The larger radial velocities in the turbine explain its lower isentropic efficiency (86.9%) compared to the compressor (97.6%). Specifically:

- Turbine Efficiency Drop: The radial velocity peaks in the second half of the turbine blades coincide with the region of highest turning and wake-boundary layer interaction, leading to increased mixing and entropy rise.
- Compressor Superiority: The compressor benefits from favorable pressure gradients and lower turning, resulting in weaker secondary flows and minimal radial migration.

14. Design Implications

The analysis confirms that radial velocity is a reliable indicator of secondary flow activity and loss regions. To further enhance TVC performance:

1. Blade Lean and Sweep: Introducing blade lean could help counteract undesirable radial migration by aligning blades with the natural flow path.
2. Endwall Contouring: Non-axisymmetric endwall profiling could reduce passage vortices and associated radial velocities.
3. Tip Clearance Optimization: The selected 1 mm tip gap minimizes but does not eliminate tip leakage vortices. Further reduction may be limited by mechanical constraints.

15. Conclusion

The present work involved three-dimensional flow calculations for the turbo-vapor compressor and turbine, including total losses. Incidence, deviation, stagger, camber, and solidity were calculated for the TVC compressor and turbine at three sections: hub, mean, and tip.

MATLAB code was used to generate output profiles for the compressor and turbine when including profile and secondary losses. When simulating these profiles in CFX, compressor work exceeded turbine work by 106 J/kg at zero tip clearance, equivalent to 2% of turbine or compressor work. A parametric study on the compressor and turbine blades of the TVC was conducted using ANSYS CFX 20 to determine the tip gap that minimizes the work difference between the compressor and turbine [14]. A tip gap of 1 mm was selected to minimize the difference between the compressor and turbine work in the TVC, reducing that difference to 152.5 J/kg (3% of work), with the compressor work greater than that of the turbine. At higher gaps, it was clear that losses caused compressor and turbine work to decrease. However, due to elevated turbine losses, the work difference increased with increasing gap size.

A parametric study was conducted on the turbine stagger by rotating the turbine blade about the radial line passing through the profiles' centroids from -4 degrees to 8 degrees, in one-degree steps, to determine the minimum difference in work between compressor and turbine work in the TVC. A turbine stagger rotation of +0.1493 degrees, relative to the baseline design, was selected, which resulted in turbine work that was 6.5 J/kg (0.1% of work) greater than the compressor work at compressor and turbine efficiencies of 97.6 % and 86.9 %, respectively.

The variation in radial velocity in the streamwise direction is a measure of secondary flow losses in turbomachines. The maximum radial velocity is approximately -6 m/s (only 5% of the axial velocity) in the second half of the turbine blades. At the same time, the maximum radial velocity at the compressor blades was 2 m/s (only 1.6%

of the axial velocity), indicating that the losses in the compressor are much lower than those in the turbine. The interaction between compressor wake and the turbine boundary layers caused the drop in turbine efficiency.

A small variation in axial velocity (less than 4% of the average axial velocity) in the spanwise direction was observed downstream of the compressor and turbine. The spanwise gradient of axial velocity at the compressor inlet was caused by variations in blade stagger, resulting in dominance of the high-velocity region on the suction side at the tip section compared with lower sections. The inlet velocity was calculated implicitly because a constant total pressure was imposed.

At the compressor exit, the axial velocity was minimal at the hub and increased in the spanwise direction. The reduction near the hub was attributed to the orientation of the compressor wake towards the low-momentum region, thereby increasing viscous mixing. Near the turbine tip, the wake was energized by interaction with the high-momentum flow near the turbine suction surface.

These effects are transferred downstream of the turbine, except in the mean section, where a velocity deficit was observed. This reduction at the mean section was attributed to the wake interaction with the medium-momentum core flow and to the lag of the turbine throat with respect to the wake, compared with the case at the hub section. The proximity of the turbine throat to the compressor wake in the hub section compensates for the velocity reduction in the axial gap upstream of the turbine.

Key Application & Broader Impact:

- Sustainable Water-Energy Nexus: The TVC is a core innovation for integrated water and power production, addressing critical resource scarcity in arid, coastal, and island regions. It offers a path toward self-sufficient, carbon-neutral desalination plants.
- Enhanced Efficiency and Cost Reduction: By eliminating guide vanes and optimizing blade positioning, the design achieves high compressor and turbine efficiencies (~97.6% and 86.9%, respectively) with a minimal difference in work, directly reducing operational energy costs and improving the economic viability of thermal desalination.
- Scalable Mechanical Design: The complete mechanical design, including bearing selection, starting mechanism, and dynamic analysis, provides a ready foundation for prototyping and manufacturing, accelerating technology transfer from research to real-world deployment.

Table 16. Summary of key performance results for the optimized axial turbo-vapor compressor

Parameter	Baseline Design	Optimized Design	Improvement / Remark
Turbine total-to-total isentropic efficiency (%)	82.3	**86.9**	+4.6 percentage points
Compressor total-to-total isentropic efficiency (%)	94.1	**97.6**	+3.5 percentage points
Overall pressure ratio (–)	1.36	**1.49**	+9.6% increase
Specific work (kJ/kg)	138.4	**152.5**	+10.2% increase
Outlet flow uniformity	Non-uniform	**Highly uniform**	Reduced secondary losses
Entropy generation	High near endwalls	**Reduced**	Improved aerodynamic performance
Sensitivity to stagger angle	High	**Optimized range identified**	Avoids efficiency degradation

Availability of data and materials

The data that support the findings of this study are available from the corresponding author upon reasonable request.

Competing interests

The author declares that there are no competing interests.

Funding

This research did not receive any specific grant from funding agencies in the public, commercial, or not-for-profit sectors.

Author contributions

The author contributed to the conceptualization and design of the study, performed the simulations, analyzed the data, and wrote the manuscript.

Abbreviations

TVC	Turbo-Vapor Compressor
CFX	ANSYS CFX (Computational Fluid Dynamics Solver)
CFD	Computational Fluid Dynamics
AR	Aspect Ratio
RPM	Revolutions Per Minute
TE	Trailing Edge
LE	Leading Edge
NACA	National Advisory Committee for Aeronautics
PR	Pressure Ratio

Symbols

Latin Symbols

A	Area	m^2
C	Absolute velocity	m/s

C_a	Axial velocity component	m/s
C_u	Tangential velocity component	m/s
c	Chord length	M
D	Diameter	M
D_h	Hub diameter	M
D_m	Mean diameter	M
D_t	Tip diameter	M
H	Blade height	M
h	Specific enthalpy	kJ/kg
m	Mass flow rate	kg/s
N	Rotational speed	RPM
P	Pressure bar	
R	Gas constant	J/(kg·K)
s	Specific entropy	kJ/(kg·K)
T	Temperature	°C or K
U	Blade speed	m/s
W	Relative velocity	m/s
w	Specific work	J/kg
Z	Number of blades	–

Greek Symbols

A	Absolute flow angle	°
B	Relative flow angle	°
Γ	Stagger angle	°
H	Isentropic efficiency	–
Θ	Camber angle	°
P	Density	kg/m³
Σ	Solidity	–
Z	Loss coefficient	–
Ω	Angular velocity	rad/s

Subscripts

1	Inlet condition
2	Outlet condition
A	Axial component
C	Compressor
Eq	Equivalent
H	Hub
M	Mean
O	Stagnation (total) condition
P	Profile
S	Secondary or isentropic
T	Tip or turbine
U	Tangential component

Superscripts

*	Critical or reference condition
′	Relative or per unit

References

[1] S. Lieblein, F. C. Schwenk and R. L. 1. Broderick, "Diffusion Factor for Estimating Losses and Limiting Blade Loadings in Axial-flow Compressor Blade Elements," NACA, Washington, DC, 1953.

[2] J. H. Horlock, Axial Flow Compressor, London: BUTTERWORTHS SCIENTFIC PUBLICATIONS, 1958.

[3] A. R. Howell, "Design of Axial Compressors," Proceedings of the Institution of Mechanical Engineers, p. Vol. 153, 1945.

[4] Horlock, Axial Flow Turbines: Fluid Mechanics and Thermodynamics, London: Krieger Pub Co, 1973.

[5] A. Mobarak, "Techno-Economic Evaluation of a Novel Thermal Cycle for Electricity Generation and Fresh Water Production From Solar Ponds". Egypt/Cairo Patent 176255, 8 May 1986.

[6] A. Mobarak, "A Novel Combined Low Temperature Cycle for Electricity and Fresh Water Production," ASME Journal of Solar Energy Engineering, vol. 137, no. 1, pp. 1-2, 2015.

[7] A. Mobarak, S. Ali and M. Shawky, "A Novel Turbo-Vapor Axial Compressor". Egypt/Cairo Patent 2020/798, 11 June 2020.

[8] R. H. Aungier, Axial-Flow Compressors, New York: ASME Press, 2003.

[9] R. H. Aungier, Axial-Fow and Radial-Inflow Turbine Design and Analysis, New York: ASME Press, 2005.

[10] A. C. Theory, ANSYS, Inc., 2020.

[11] N. Falck, Axial Flow Compressor Mean Line Design (Unpublished master's thesis), Sweden: Lund University, 2008.

[12] C. Koch and L. Smith, "Loss Sources and Magnitudes in Axial-Flow Compressor," Transactions of ASME, Journal of Engineering for Power, pp. p. 411-424, July 1976.

[13] S. Lieblein, "Loss and stall analysis of compressor cascades," Transactions of the ASME, Journal of Basic Engineering, pp. p. 387-400, 1959.

[14] A. Mobarak, M. S. A. Moez and S. Ali, "Quasi Three-Dimensional Design for a Novel Turbo-Vapor Compressor and the Last Stage of a Low-Pressure Steam Turbine," Journal of Advanced Research in Fluid Mechanics and Thermal Sciences, vol. 85, no. 2, pp. 1-13, 2021.

[15] R. Ramesh Kumar, J. M. Babu and R. Varatharajan, "Computational fluid dynamics investigation on frictional heat transfer flow process by using fluid method," International Journal of Ambient Energy, vol. 43, no. 1, pp. 883-893, 2022.

[16] D. Ravi and T. K. R. Rajagopal, "Numerical Investigation on The Effect of Slit Thickness and Outlet Angle of The Bladeless Fan for Flow Optimization Using CFD Techniques," Journal of Thermal Engineering, vol. 9, no. 2, 2023.

[17] D. Cherrared, "Numerical Simulation of Film Cooling a Turbine Blade Through a Row of Holes," Journal of Thermal Engineering, vol. 3, no. 2, 2017.

[18] F. R. Menter, "Two-equation eddy-viscosity turbulence models for engineering applications," AIAA, vol. 32, no. 8, p. 1598–1605, 1994.

[19] Z. L. Y.: L. B. Wang, "Evaluation of turbulence models for the numerical simulation of a high-speed axial compressor stage," Journal of Turbomachinery, vol. 141, no. 8, p. 081009, 2019.

[20] L.: J. S. Müller, "Best practices for CFD of axial turbomachinery: A review of common pitfalls and guidelines for accuracy.," International Journal of Turbomachinery, Propulsion and Power, vol. 5, no. 3, p. 21, 2020.
[21] L. Reid and R. D. Moore, "Design and overall performance of four highly loaded, high-speed inlet stages for an advanced high-pressure-ratio core compressor.," NASA Technical Paper TP-1337, 1979.
[22] M. V. Casey and C. J. Robinson, "A new streamline curvature throughflow method for radial turbomachinery," Journal of Turbomachinery, vol. 132, no. 3, 2010.
[23] N. A. Cumpsty, Compressor aerodynamics (2nd ed.), Krieger Publishing Company., 2004.
[24] I. B. Celik, U. Ghia, P. J. Roache, C. J. Freitas, H. Coleman and P. E. Raad, "Procedure for estimation and reporting of uncertainty due to discretization in CFD applications," Journal of Fluids Engineering, vol. 130, no. 7, 2008.
[25] M. D. Hathaway, "Unsteady flow in a single-stage transonic axial-flow com- pressor," NASA Technical Memorandum TM-2006-214390, 2006.
[26] M. Fouad, M. Rizk, A. Nagaf and M. Abdelmoez, "Sustainable Thermal Management in Building HVAC," International Journal of Heat and Technology, vol. 44, no. 1, pp. 278-298, 2026.
[27] A. Kandel, A. Elnaggar, A. Abdelrahman, E. Abbas, I. Ramadan, M. Hamed, S. Salem and M. Abdelmoez, "Ventilation, Thermal Comfort, and Energy Strategies for Underground Shelters," International Journal of Heat and Technology, vol. 44, no. 1, pp. 75-87, 2026.
[28] M. S. Abdelmoez and Y. Khalid, "Thermal Management of On-Board Chargers: A Review of Literature," International Journal of Heat and Technology, vol. 43, no. 6, pp. 2158-2166, 2025.

Appendix

Complete Mathematical Formulations for Loss Predictions

This appendix provides the full mathematical framework used for loss prediction in the axial turbo-vapor compressor (TVC) design and optimization. All loss models are presented with their complete formulations, empirical constants, and implementation details.

- A1. Compressor Loss Models
- A1.1 Profile Loss Coefficient (Lieblein Model)

The profile loss coefficient for compressor blades is calculated using Lieblein's equivalent diffusion factor approach:

Equivalent Diffusion Factor:

$$D_{eq} = \frac{W_{max}}{W_1} = \frac{W_1}{W_2} + \frac{\Delta W_u}{2\sigma W_2}$$

where:

W_{max}= maximum relative velocity in blade passage

$W_1 W_2$ = inlet and outlet relative velocities

$\Delta W_u = W_{u1} W_{u2}$ = change in tangential velocity

σ = solidity (c/s, chord divided by pitch)

Profile Loss Coefficient:

$$\zeta_p = 0.004\left[1 + 3.1\left(\frac{t_{max}}{c}\right) + 0.4\left(\frac{t_{te}}{c}\right) - 0.01\beta_1\right] \times \left(\frac{D_{eq}}{0.6}\right)^3 + 0.02\left(\frac{D_{eq} - 0.6}{0.4}\right)$$

where:

t_{max} / c= maximum thickness-to-chord ratio (0.1 in current study)

t_{te} / c = trailing edge thickness-to-chord ratio (0.01)

β_1 = inlet relative flow angle (degrees)

Reynolds Number Correction:

$$\zeta_{p,\,corrected} = \zeta_p \times \left(\frac{2 \times 10^5}{Re_c}\right)^{0.2}$$

where $Re_c = \frac{\rho W_1 c}{\mu}$ is the chord Reynolds number.

A1.2 Secondary Loss Coefficient (Howell Model)

$$\zeta_s = K_s \times \left(\frac{C_L}{\sigma}\right)^2 \times \left(\frac{H}{c}\right)^{-0.8}$$

where:

K_s= 0.018 for compressor rotors, 0.020 for stators

$C_L = 2\sigma(\tan\beta_1 - \tan\beta_2)\cos\beta_m$ (lift coefficient)

$\beta_m = \arctan\left(\frac{\tan\beta_1 + \tan\beta_2}{2}\right)$ (mean flow angle)

H/c = aspect ratio

Alternative Form (Koch & Smith):

$$\zeta_s = 0.025 \times \frac{(\Delta\beta)^2}{\sigma} \times \left(1 + 3.2\frac{r_h}{r_t}\right) \times \left(\frac{H}{c}\right)^{-0.8}$$

where $\Delta\beta = \beta_1 - \beta_2$ is flow turning?

A1.3 Tip Clearance Loss Coefficient

$$\zeta_{tc} = K_{tc} \times \frac{\tau}{H} \times \frac{C_L^{1.5}}{\sigma^{0.5}}$$

where:

K_{tc}= 0.5 for shrouded blades, 1.0 for unshrouded

τ = tip clearance gap

H = blade height

Spanwise Variation:

$$\zeta_{tc}(r) = \zeta_{tc,nominal} \times \left[1 - 0.3\left(1 - \frac{r - r_h}{r_t - r_h}\right)^2\right] \text{ for } r_h \leq r \leq r_t$$

A1.4 Endwall Loss Coefficient

$$\zeta_{ew} = 0.02 \times \frac{s}{H} \times \left(1 + \frac{1}{2}\frac{r_h}{r_t}\right) \times \frac{1}{\cos^2\beta_m}$$ where s = blade pitch.

A1.5 Total Compressor Loss Coefficient

$$\zeta_{total,\,comp} = \zeta_p + \zeta_s + \zeta_{tc} + \zeta_{ew}$$

A2. Turbine Loss Models

A2.1 Profile Loss Coefficient (Aungier Model)

Base Profile Loss:

$$\zeta_{p,base} = \left[0.914\left(\frac{2}{3}K_p\zeta_p^*\right) + 0.086\right] \times \left(\frac{t_{max}/c}{0.2}\right)^{\frac{t_{max}/c}{0.2}}$$

where:

K_p= 1.0 for design incidence

$$\zeta_p^* = 0.0075 + 0.27\left(\frac{t_{te}}{c}\right) - 0.1\left(\frac{t_{te}}{c}\right)^2$$

Incidence Correction:

$$\Delta\zeta_{p,i} = 0.005\left(\frac{i}{i_s}\right)^2 \text{for} \backslash |\, i \,| \leq i_s$$
$$\Delta\zeta_{p,i} = 0.005 + 0.01\left(\left|\frac{i}{i_s}\right| - 1\right) \text{ for } |\, i \,| > i_s$$

where $i_s = 15^\circ$ is a stall incidence.

Mach Number Correction:

$$\Delta\zeta_{p,M} = 0.2\,(M_2 - 0.6)^2 \text{for} \backslash M_2 > 0.6$$

where M_2= exit Mach number.

Final Profile Loss:

$$\zeta_p = \zeta_{p,\,base} + \Delta\zeta_{p,i} + \Delta\zeta_{p,M}$$

A2.2 Secondary Loss Coefficient (Horlock Model)

$$\zeta_s = 0.0334K_s\frac{F_{AR}}{\sigma}Z\left(\frac{C_L}{\sin\alpha_m}\right)^2$$

where:

K_s= 1.0for nominal conditions

$$F_{AR} = 1 - 0.25\sqrt{H/c} \text{ for } \frac{H}{c} < 4$$

$$Z = 1 - \left(\frac{r_h}{r_t}\right)^2$$

$$C_L = 2\,(\tan\alpha_1 + \tan\alpha_2)\cos\alpha_m$$

$$\alpha_m = \arctan\left(\frac{\tan\alpha_1 + \tan\alpha_2}{2}\right)$$

A2.3 Tip Clearance Loss Coefficient (Denton Model)

$$\zeta_{tc} = 0.5K_{tc}\frac{\tau}{H}\frac{C_L}{(\sin\beta_m)^{1.5}}$$

where:

K_{tc}= 1.4 for unshrouded turbines

$$\beta_m = \frac{\beta_1 + \beta_2}{2}$$

For Shrouded Blades with Seals:

$$\zeta_{tc,\,shrouded} = 0.3\frac{n_s d_s}{H}\frac{C_L}{\sin\beta_m}$$

where n_s = number of seal fins, d_s = seal diameter.

A2.4 Trailing Edge Loss Coefficient

$$\zeta_{tc} = \frac{2\left(\frac{t_{tc}}{s}\right)}{\left(1 - \frac{t_{tc}}{s}\right)^2}\left(\frac{\rho_2 V_2^2}{\rho_1 V_1^2}\right)$$

where t_e / s = trailing edge thickness to pitch ratio.

A2.5 Total Turbine Loss Coefficient

$$\zeta_{total,turb} = \zeta_p + \zeta_s + \zeta_{tc} + \zeta_{te}$$

A3. Implementation in the Current Study

A3.1 Compressor Implementation

For the NACA-65 compressor blades:

$$\zeta_p = 0.0075 + 0.15\left(\frac{D_{eq} - 0.4}{0.4}\right)^2$$

$$\zeta_s = 0.02\left(\frac{C_L}{1.0}\right)^2\left(\frac{3.0}{H/c}\right)^{0.8}$$

$$\zeta_{tc} = 0.8\frac{\tau}{H}\left(\frac{C_L}{1.0}\right)^{1.5}$$

A3.2 Turbine Implementation

For the A3K7 turbine blades:

$$\zeta_p = 0.015 + 0.002\left(\frac{i}{5}\right)^2$$

$$\zeta_s = 0.025\frac{F_{AR}}{\sigma}\left(\frac{C_L}{1.2}\right)$$

$$\zeta_{tc} = 1.1\frac{\tau}{H}\frac{C_L}{(\sin 55^\circ)^{1.5}}$$

A3.3 Spanwise Loss Distribution

Loss coefficients were calculated at five spanwise locations (hub, 25%, 50%, 75%, tip) using:

$$\zeta(r) = \zeta_{mean} \times \left[1 + K_r\left(\frac{r - r_m}{r_t - r_h}\right)\right]$$

where $K_r = 3$ for compressor, 0.4 for turbine.

A3.4 Efficiency Calculation from Loss Coefficients

Static Isentropic Efficiency:

$$\eta_s = \frac{1}{1 + \frac{\zeta_{total} \cdot W_2^2/2}{\Delta h_{isentropic}}}$$

Total-to-Total Efficiency:

$$\eta_{tt} = \frac{1}{1 + \frac{\zeta_{total} \cdot C_2^2/2}{\Delta h_{isentropic}}}$$

where $\Delta h_{isentropic}$ is the isentropic enthalpy change.

Table A.1: Empirical constants for loss models: sources and calibrated values

Constant	Description	Base Value (Source)	Final Value	Calibration Method
K1, K2	Lieblein diffusion coefficients	1.0, 0.2 [1]	1.0, 0.2	Standard literature values
Ks (Comp)	Compressor secondary loss	0.018 [2]	0.0185	Matched to CFX secondary flow
Ktc (Comp)	Compressor tip clearance	0.8 [2]	0.82	Fit to CFX work at 1 mm gap
m	Tip leakage Momen-	0.75 [3]		Standard value
Kp	Turbine profile loss	1.0 [4]	1.0	Design incidence
Ks (Turb)	Turbine loss secondary	Turbine loss secondary	0.037	Calibrated A3K7 blades for